PSR B1929+10 REVISITED IN X-RAYS

A. WOŹNA[1,2], L. KUIPER[3], W. HERMSEN[3]
[1] *Max Planck Institute for Extraterrestrial Physics, Garching, Germany*
[2] *Nicolaus Copernicus Astronomical Center, Toruń,Poland*
[3] *Space Research Organization Netherlands, Utrecht, The Netherlands*

ABSTRACT. We performed timing and spectral analysis for PSR B1929+10, one of the oldest (about 10^7 years) of the ordinary pulsars detected in X-rays, using archival ROSAT, ASCA and RXTE data. Pulsed emission was detected at a more than five sigma level for combined ROSAT PSPC and unpublished HRI data. Our pulse profile is in agreement with that obtained by Yancopoulos et al. (1994; ROSAT PSPC) but now with better statistics. An investigation of the behaviour of the pulsed signal as a function of energy , based on PSPC data, provides indications that the pulsed fraction is changing with energy. The most important new result from this work is derived from the spectral analysis. We found that the combined ROSAT PSPC and ASCA GIS spectrum can satisfactorily be described by a power-law as well as by a double black-body model but not by a single black-body model, as was presented earlier by Yancopoulos et al. (1994; ROSAT) and Wang et al. (1997; ASCA). Fitting the combined ROSAT/ASCA 0.1 - 10 keV spectrum by a power-law model we obtain a photon index of 2.54 ± 0.12 and a neutral Hydrogen column density (N_H) towards the source of $9.8^{+1.4}_{-1.0} \cdot 10^{20}$ cm^{-2}. For a double black-body fit our results are: $T_1 = 2.0^{+0.05}_{-0.05} \cdot 10^6$ K, $T_2 = 6.9^{+0.23}_{-0.35} \cdot 10^6$ K, and $N_H = 4.43^{+2.08}_{-1.12} \cdot 10^{20}$ cm^{-2}. In both cases the derived N_H value is higher than that adopted in earlier works, but our result is consistent with the larger distance estimate of 331 ± 10 pc from new parallax measurements performed by Brisken et al. (2002) and with the Hydrogen distribution measured in the direction of the pulsar (Frisch & York, 1983). No significant pulsed signal is found in the RXTE data.

1. Introduction

PSR B1929+10 is one of the closest and oldest known ordinary pulsars that has been detected in X-rays. The two latest investigations of this object in X-rays were based on ROSAT PSPC (Yancopoulos et al. 1994, hereafter Y94) and ASCA (Wang & Halpern 1997, hereafter WH97) observations with exposure durations of 45 ks and 54 ks, respectively. Y94 obtained, after background subtraction, a total of 420 ± 25 photons in the 0.1 - 2.0 keV band, corresponding to a luminosity of $1.2 \cdot 10^{30}$ ergs s^{-1} for a source distance of 250 pc, or $\sim 3 \cdot 10^{-4}$ of the pulsar's spin-down luminosity. After folding the barycentered arrival times of the selected events Y94 fitted the pulse shape using a sinusoid yielding a pulsed fraction of 0.28 ± 0.10. The spectrum was fitted with a black-body with temperature $T_\infty \approx 3.2 \cdot 10^6$ K, which indicated that the implied emitting area has a radius of less than 50 m. WH97 used ASCA data from October 1994. The spectrum of PSR B1929+10 over the 0.5 - 5.0 keV range was fitted with a single black-body. The neutral Hydrogen column density was not included as a free parameter in the fit. It was fixed at the level $\sim 1 \cdot 10^{20}$ cm^{-2}, and the luminosity was calculated for a distance of 250 pc used by Y94. Their results yield $T = 5.14 \pm 0.53 \cdot 10^6$ K and $L \approx 1.28 \cdot 10^{30}$ ergs s^{-1}. In the timing analysis WH97 extracted events from a circle of radius 2.5 arcmin for both GIS 2 and 3 and obtained 747 counts within this radius, 413 of which were estimated to belong to the background. The lightcurve was characterized by a single broad maximum, similar to the ROSAT soft X-ray profile, with a modulation significance of $\sim 3.1\ \sigma$. The pulse fraction was estimated to be 0.35 ± 0.15. Both groups were unable to discriminate conclusively between a thermal and a non-thermal spectrum. While a black-body is a better overall fit, the inferred emitting area is surprisingly small.

In this study we revisited the ROSAT PSPC and ASCA analyses. Moreover, we also included ROSAT HRI data from a combination of 3 observations lasting 346 ks in total, together with data from a 30 ks RXTE exposure. The main goal was to characterize the timing and spectral properties of PSR B1929+10 in more detail using all available X-ray data.

2. Observations

In our study we made use of archival ROSAT PSPC/HRI, ASCA SIS/GIS and RXTE PCA data. An overview of the X-ray observations of PSR B1929+10 is presented in Table I.

TABLE I
X-ray observations of PSR B1929+10

Instrument	ROSAT			
Detector	PSPC	HRI		
Obs. start	30/03/91	09/10/95	02/10/96	13/04/97
Obs. end	25/04/91	07/11/95	21/10/96	28/04/97
On - Time (ks)	43.57	104.125	136.598	106.019

Instrument	ASCA		RXTE
Detector	GIS	SIS	PCA
Obs. start	17/10/94	17/10/94	21/11/97
Obs. end	19/10/94	19/10/94	21/11/97
On - Time (ks)	56.448	53.323	29.65

3. Timing analysis

3.1. ROSAT PSPC

Point-like X-ray emission was clearly detected in the vicinity of the radio position of the pulsar on the ROSAT PSPC Maximum Likelihood Ratio map (MLR map, see e.g. Kuiper et al. 1998). The number of source and background counts are derived simultaneously by this method. In the timing analysis we extracted events within an optimum radius (the radius where the signal-to-noise ratio S/N maximizes) of $50''$ from the X-ray centroid. The 604 events (0.1 - 2.5 keV) falling within this radius have subsequently been barycentered and folded through appropriate pulsar parameters (see e.g. Table II for general characteristics of PSR B1929+10) to obtain the pulse-phase distribution shown in left panel of Fig. 1. The profile is characterized by one broad maximum and deviates from a statistically flat distribution at a 4.2 σ level when applying a Z_1^1 method (Buccheri et al. 1983). Due to the limited accuracy of the ROSAT absolute timing we could not relate the X-ray phase to the radio phase. In order to quantify the pulsed fraction we have applied two methods: one based on bootstrapping (Swanepoel et al. 1996) and another based on sinusoid fitting. For broad sinusoidal profiles it is expected that the bootstrap method will systematically underestimate the genuine pulsed fraction because parts of the leading and trailing wings of the broad profile are considered to be part of the interval used to construct the unpulsed level. Applying the bootstrap method we obtain a pulsed fraction, defined as $f_{pulsed} = \frac{N_P}{N_P+N_{DC}}$, of 0.24 ± 0.07. The number of pulsed counts N_P follows directly from the bootstrap method, while the number of DC counts N_{DC} requires an estimate of the number of background counts within the extraction radius of $50''$. From the MLR map we could estimate that 140.5 ± 2.2 background

counts are expected within the extraction radius.

TABLE II
Pulsar characteristics[a]

Parameter	Value
PSR	B1929+10 ≡ J1932+1059
Right Ascension (J2000)	$19^{\rm h}\ 32^{\rm m}\ 13^{\rm s}.899$
Declination (J2000)	$10^\circ\ 59'\ 31''.99$
Period	0.226518 s
Period derivative	$1.15661 \cdot 10^{-15}$
Age	3.1 Myr
Magnetic field[b]	$0.51 \cdot 10^{12}$ G
Distance[c]	331 pc
Spin–down luminosity[d]	$3.89 \cdot 10^{33}$ ergs s^{-1}

[a] Taylor et al. 1993.
[b] $B = (3Ic^3P\dot{P}/8\pi^2R^6)^{1/2}$, for $R = 10^6$ cm, $I = 10^{45}$ g cm^2.
[c] From parallax measurements by Brisken et al. 2002.
[d] $\dot{E} = 4\pi^2 I\dot{P}P^{-3}$, for $I = 10^{45}$ g cm^2.

Because the pulse profile shows one broad maximum sinusoid fitting using one harmonic provides an adequate description of the measured distribution. Applying sinusoid fitting to the 0.1 - 2.5 keV PSPC pulse profile (see Fig. 2 *left panel*) we find a pulse fraction of 0.36 ± 0.08 slightly higher than the bootstrap value, as expected, and consistent with the value found earlier by Y94.

By selecting the events further on energy we applied the same sinusoid fitting method to the 0.1 - 1.28 keV and 1.28 - 2.5 keV pulse profiles. These two profiles are also shown in Fig. 1: 0.1 - 1.28 keV, *middle panel*; modulation significance 3.0 σ, and 1.28 - 2.5 keV, *right panel*, modulation significance also 3.0 σ. The pulsed fractions applying sinusoid fitting for these energy ranges are 0.33 ± 0.09 and 0.42 ± 0.13, respectively.

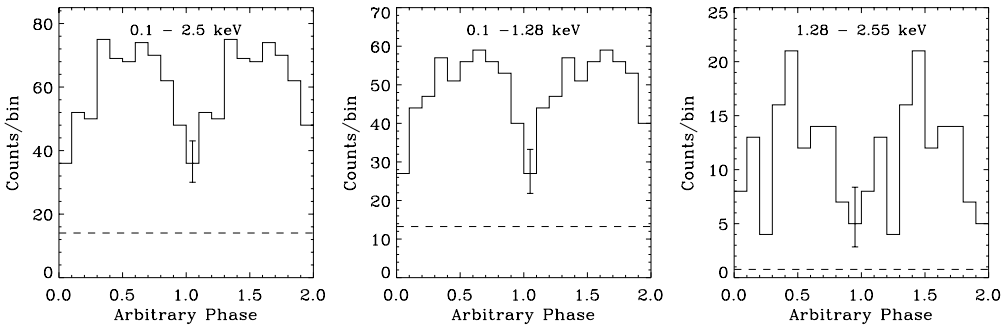

Fig. 1. PSR B1929+10 phase histograms from ROSAT PSPC data in three energy ranges, *left panel*: 0.1 - 2.5 keV, *center panel*: 0.1 - 1.28 keV, *right panel*: 1.28 - 2.5 keV. Two cycles are shown for clarity. A typical error bar is shown on each panel. The significance for a deviation from a statistically flat distribution is 4.15 σ (604 events), 3.0 σ (490 events), 3.0 σ (114 events), respectively.

3.2. ROSAT HRI

For the 3 long ROSAT HRI observations (see Table I) the timing analysis consisted in extracting the events from a 11″ aperture around the centroid of the PSR B1929+10

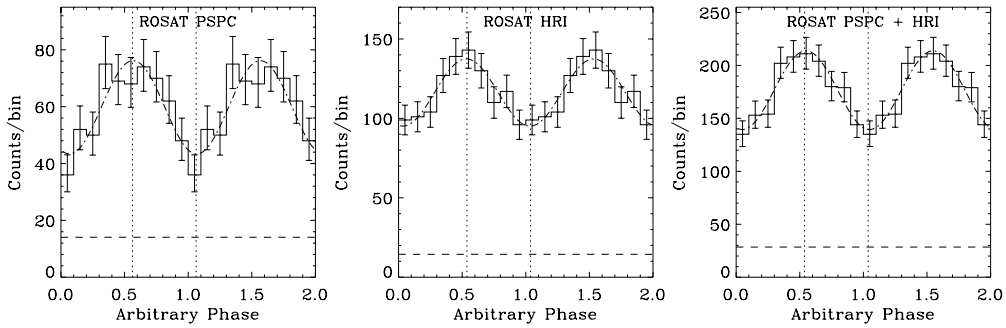

Fig. 2. Light curves for the ROSAT PSPC and HRI observations of PSR B1929+10. *Left panel*: only PSPC (0.1 - 2.5 keV), *center panel*: only HRI (0.1 - 2.4 keV), *right panel*: combined PSPC and HRI. Two cycles are shown for clarity. Error bars are shown in each panel. The significance for a deviation from a statistically flat distribution is 4.15 σ, 3.7 σ and 5.6 σ, respectively. The dashed horizontal lines indicate the background level determined from a spatial analysis. The vertical dotted lines correspond to minimum and maximum phase of the sinusoid function fit (dot - dashed curve).

counterpart and subsequently folding the barycentered event times using an appropriate pulsar ephemeris. The obtained pulse profiles for each observation are all of low significance (between 2 - 3 sigma), although the broad bump can be discerned easily. Cross-correlating each of the three HRI profiles with the 0.1 - 2.5 keV PSPC profile and applying the shifts in the combination of the three separate aligned profiles, yielded a phase distribution which deviates from a flat distribution at the 3.7 σ level (see Fig. 2 *middle panel*). In this case the sinusoid fitting method yielded a pulsed fraction of 0.21 ± 0.05, lower but consistent with the PSPC value. The combined ROSAT PSPC and HRI profile is shown in the *right panel* of Fig. 2 and it deviates from being flat at a 5.6 σ level. The pulsed fraction of the combined profile is 0.25 ± 0.04.

3.3. ASCA GIS

Of the two detector systems aboard ASCA only the GIS detectors have sufficient timing resolution to support timing analyses at millisecond scales. Data from the high and medium rate telemetry mode were used. The 3.9 ms timing resolution valid for these rates was sufficiently high to sample the pulse period of 227 ms (see Table II). In the spatial analysis a Maximum Likelihood method similar to the one used for the ROSAT PSPC/HRI data, provided the optimum position for the X-ray counterpart of PSR B1929+10. An extraction radius of 130″ from the optimum position was found to optimize the S/N ratio. In the 0.5 - 5 keV energy interval 493 event timetags were barycentered and subsequently folded through appropriate timing parameters to yield the corresponding pulse profile. This 0.5 - 5 keV profile is shown in Fig. 3 *left panel* and deviates from uniformity at a 2.7 σ level. The same broad enhancement is visible as in the ROSAT profiles at softer X-ray energies. Constraining the energy to the 0.5 - 2.0 keV interval, fully overlapping the ROSAT energy window, yielded a significance of 3.1 σ (see Fig. 3 *right panel*). The pulsed fractions derived from sinusoid fitting for the (integral) 0.5 - 5 keV and (ROSAT overlapping) 0.5 - 2.0 keV energy ranges are 0.36 ± 0.11 and 0.69 ± 0.18, respectively. The former value is consistent with the one found by W97, while the latter value derived for the ROSAT overlapping interval seems to confirm the increasing trend seen at soft X-ray energies for the pulsed fraction as a function of energy.

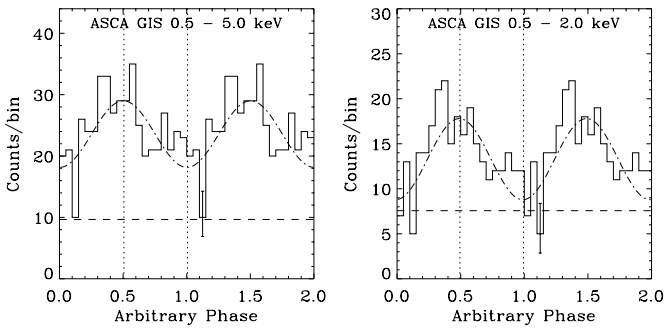

Fig. 3. The ASCA profiles of PSR B1929+10 in two energy intervals: *left panel* 0.5 - 5.0 keV (significance 2.7 σ) and *right panel* 0.5 - 2.0 keV (significance 3.1 σ). The dot - dashed curves indicate the sinusoid function fitted to the data, while the vertical dotted lines correspond to the minimum and maximum phase of these fits. In both panels the horizontal dashed lines indicate the background levels determined from a spatial analysis. A typical error bar is shown in each panel. Two cycles are shown for clarity.

3.4. RXTE PCA

Finally, we analysed RXTE PCA (2 - 60 keV) data from a 30 ks observation of PSR B1929+10 (Obs. id. 20156; 21-Nov-1997) obtained in Good Xenon mode, time tagging each event with a 0.9 μs time resolution. For the timing analysis we used ftools program fasebin to select events from the top layer of each involved PCU, to barycenter the times of the selected events and finally to fold the barycentered event times with an appropriate ephemeris. The ephemeris we used in the folding procedure within fasebin is based on radio timing observations of PSR B1929+10 with the 32m TCfA radio-telescope at Toruń, Poland since the beginning of June 1997. A dual-channel, circular polarization L-band receiving system at frequencies around 1.7 GHz and a 2 x 64 x 3 MHz pulsar back-end, the Penn Stata Pulsar Machine - 2 (Konacki et al. 1999) are used. For analyzing the radio pulsar timing data the TEMPO software package (*http://pulsar.princeton.edu/tempo*) has been used.

The folding procedure embedded in fasebin resulted in pulse phase histograms for each of the 256 PHA channels. Unfortunately, in none of the PHA channels or channel intervals significant pulsed emission has been detected.

4. Spectral analysis

In the spectral analysis we first derived the number of counts assigned to the X-ray counterpart of PSR B1929+10 in several narrow energy slices using a spatial (MLR) analysis which took into account the presence of nearby sources. We applied this approach to the ROSAT PSPC-B (20 energy bins in the interval 0.1 - 2.5 keV) and ASCA GIS 2+3 (10 energy bins in the interval 0.5 - 10 keV) data. We chose for ASCA GIS data (contrary to W97) because the GIS sensitivity is higher than the SIS sensitivity for energies beyond $\sim$ 5 keV and because of uncertainties in the SIS efficiency for energies below 1 keV. In the combined ROSAT PSPC-B and ASCA GIS 2+3 spectral fits we used the latest upgrades for the response matrices and we took into account the vignetting corrections for the off-axis (3.7 arcmin) ASCA observation. The spectral models we fitted to the combined data set consist of a single absorbed power-law, a single absorbed black-body, an absorbed black-body plus power-law and an absorbed double black-body. The best fits were obtained for a single absorbed power-law (Fig. 4 *left panel*) and an absorbed

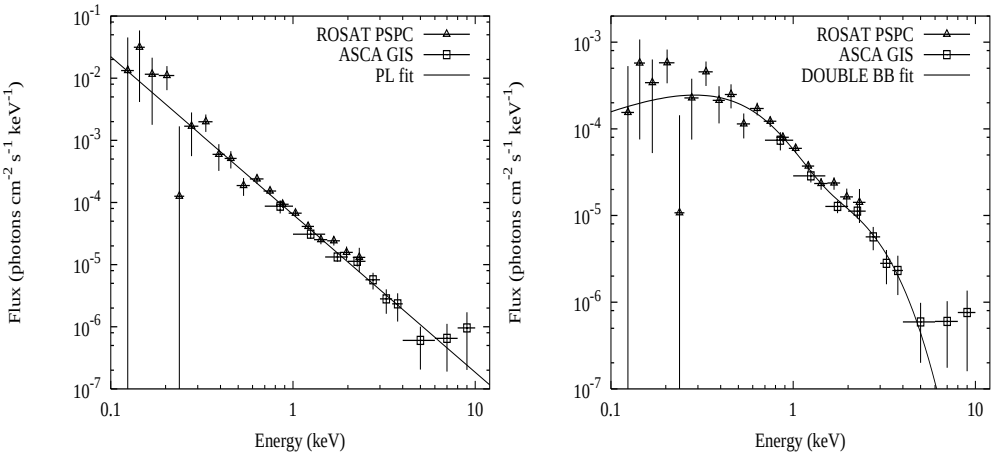

Fig. 4. 0.1 - 10 keV spectrum of PSR B1929+10 from combined ROSAT PSPC-B and ASCA GIS 2+3 data: *left panel* power-law model, *right panel* double black-body model.

double black-body model (Fig. 4 *right panel*). The fit results for the latter two cases, each with a free Hydrogen column density, are shown in Table III.

TABLE III
Fits to combined ROSAT and ASCA spectrum in the energy range 0.1 - 10 keV

Parameter	Power Law Fit	Parameter	Double Black-Body Fit
C^a	$6.41^{+0.4}_{-0.4} \cdot 10^{-5}$	C_1	$0.0117^{+0.0017}_{-0.0018}$
α	$2.54^{+0.12}_{-0.13}$	kT_1	$0.176^{+0.004}_{-0.004}$ keV
N_H	$9.8^{+1.4}_{-1.0} \cdot 10^{20}$ cm^{-2}	C_2	$7.879^{+1.32}_{-1.26} \cdot 10^{-5}$
χ^2_ν/ν	1.146/27	kT_2	$0.595^{+0.02}_{-0.03}$ keV
		N_H	$4.43^{+2.08}_{-1.12} \cdot 10^{20}$ cm^{-2}
		χ^2_ν/ν	1.132/25

[a] Normalization at 1 keV (ph cm^{-2} s^{-1} keV^{-1}).

In case of the double black-body model we are dealing with two different thermal X-ray components with temperatures $(2.0^{+0.05}_{-0.05}) \cdot 10^6$ K and $(6.9^{+0.23}_{-0.35}) \cdot 10^6$ K for T_1 and T_2, respectively. For the characteristic age of PSR B1929+10 ($\tau \simeq 3.1$ Myr) cooling models predict a surface temperature of the neutron star to be $\lesssim 10^5$ K, much too low to be responsible for the observed X-ray spectrum of PSR B1929+10. However, a plausible explanation could be that the observed X-ray radiation originates from a heated polar cap characterized by two different thermal components (see e.g. Cheng & Zhang 1999). The N_H value obtained from the fit is about two times higher than that used by Y94 and WH97. Moreover, the (non-thermal) power-law fit resulting in a photon index of 2.54 ± 0.12 yielded an estimate for the neutral Hydrogen density towards the source of $9.8^{+1.4}_{-1.0} \cdot 10^{20}$cm^{-2}. This value is six times larger than the adopted one in earlier works (Y94, WH97). In both cases the derived column density is consistent with the updated (radio) distance determined by Brisken et al. (2002), and the Hydrogen distribution measured in the direction of the pulsar (Frisch & York, 1983). Additionally, as Pavlov et al. (1996) mentioned, values of N_H obtained from direct measurements of stars in

the neighbourhood of the pulsar are rather controversial. They differ from $< 10^{19}$ up to 10^{21} cm^{-2}. This suggests that interstellar medium is very patchy in that direction.

5. Conclusion

Our revisited analysis of X-ray data of PSR 1929+10 from ROSAT, ASCA and RXTE observations yielded an improved timing signal at soft X-rays, 5.6 σ for the combined ROSAT PSPC/HRI pulse profile, and a non-detection for energies beyond $\sim$ 2 keV (RXTE PCA). Analyzing the pulse profile at soft X-rays (ROSAT PSPC) in two different energy bands suggested that the pulsed fraction increases from 0.33 ± 0.09 in the 0.1 - 1.28 keV band to 0.42 ± 0.13 in the 1.28 - 2.5 keV band (even 0.69 ± 0.18 for the 0.5 - 2 keV ASCA GIS band). This tendency must stop abruptly near $\sim$ 2 keV to be consistent with the non-detection of pulsed emission above $\sim$ 2 keV. A spectral analysis of the combined ROSAT/ASCA data in the 0.1 - 10 keV energy range indicated that both an absorbed power-law (non-thermal) model and an absorbed double black-body model provide an adequate description of the observed X-ray spectrum. The derived Hydrogen column density N_H is in both cases much larger than the value used in previous X-ray studies. However, the newly determined N_H values are more consistent with the updated (increased) distance to PSR B1929+10 in combination with the measured Hydrogen distribution in the direction of the pulsar.

A scheduled observation with the XMM-Newton satellite could confirm our results and the much better statistics would help to fix the column density N_H and to discriminate conclusively between thermal and non-thermal models for the X-ray emission from this pulsar.

Acknowledgements

This research was supported by KBN grant 2P03D02117 and Polish Foundation of Astronomy. Aga Woźna acknowledges people from SRON for their hospitality during her stay there, when most of this work was done.

References

Brisken W.F. et al.:2002, *Astrophys. J.* **571**, 906.
Buccheri R. et al.:1983, *Astron. Astrophys.* **128**, 245.
Cheng K.S. & Zhang L.:1999, *Astrophys. J.* **515**, 337.
Frisch P.C., York D. G.: 1983, *Astrophys. J. Lett.* **271**, L59.
Konacki M. et al.:1999, *Astrophys. J. Lett.* **519**, L81.
Kuiper L., et al.: 1998, *Astron. Astrophys.* **337**, 421
Pavlov G.G. et al.: 1996, *Astrophys. J.* **429**, 832.
Swanepoel J.W.H. et al.: 1996, *Astrophys. J.* **467**, 261.
Taylor J.H. et al.: 1993, *Astrophys. J. Suppl.* **88**, 529.
Yancopoulos A.H. et al.: 1994, *Astrophys. J.* **429**, 832.
Wang F.Y.-H., Halpern J. P.: 1997, *Astrophys. J. Lett.* **482**, L159.

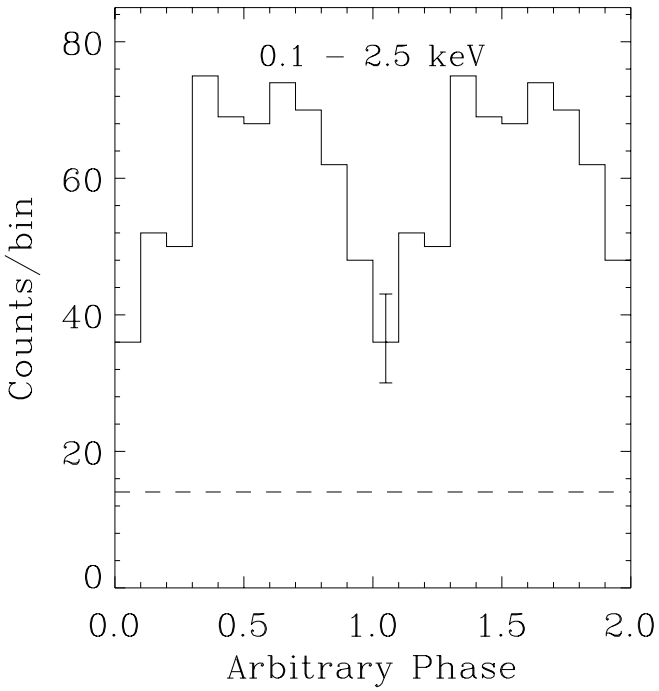
0.1 – 2.5 keV
Counts/bin
0
20
40
60
80
0.0
0.5
1.0
1.5
2.0
Arbitrary Phase

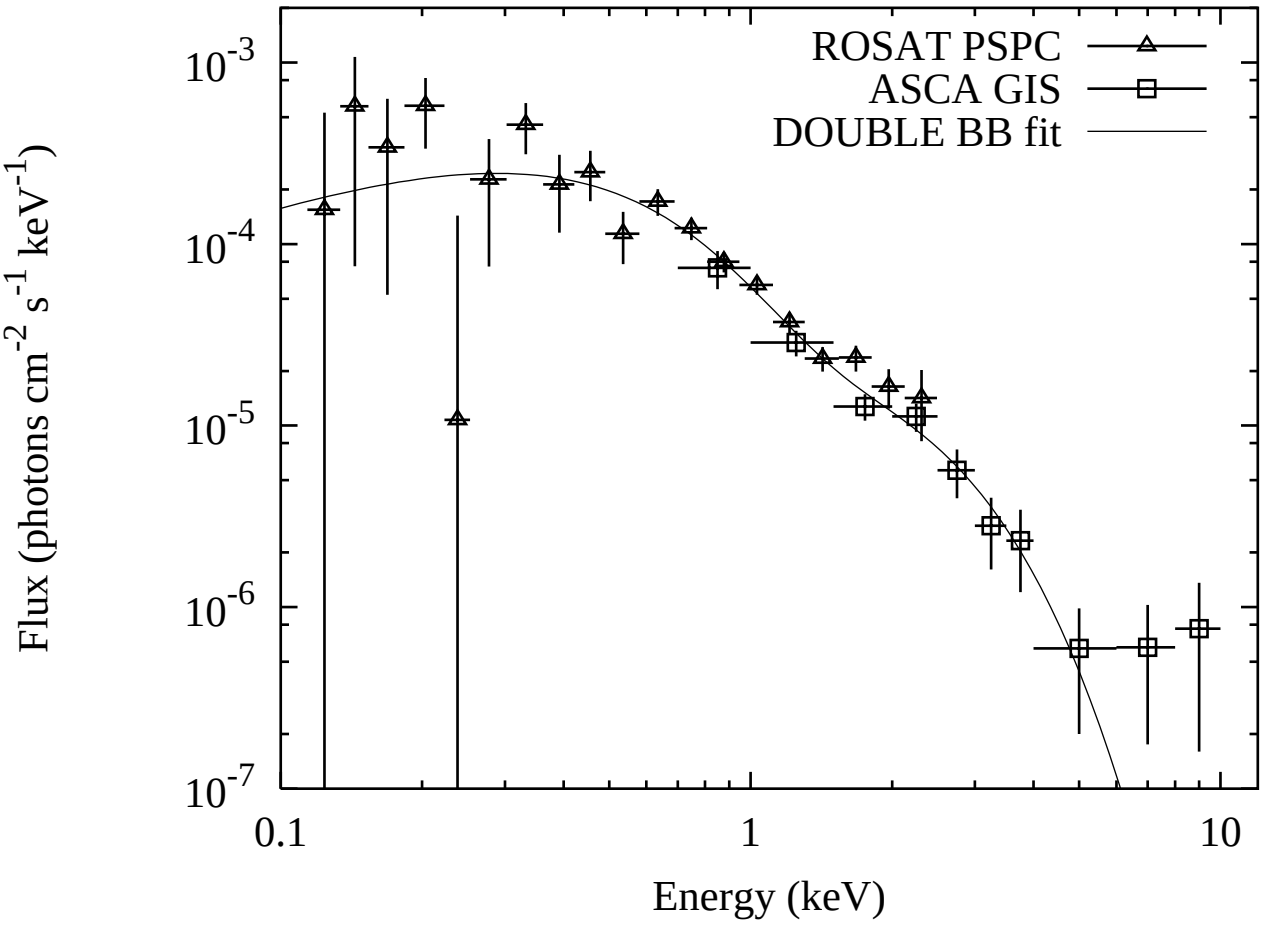
ROSAT PSPC
ASCA GIS
DOUBLE BB fit
Flux (photons cm-2 s-1 keV-1)
10-3
10-4
10-5
10-6
10-7
0.1
1
10
Energy (keV)

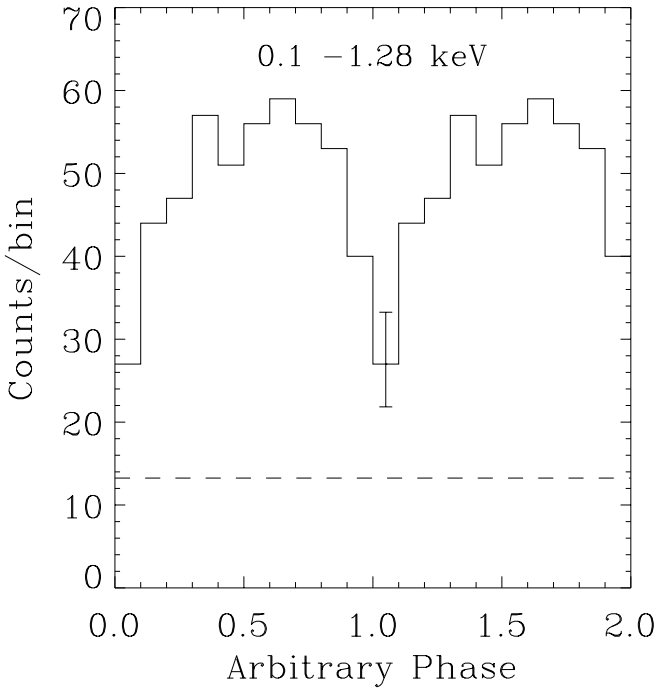
0.1 −1.28 keV
Counts/bin
Arbitrary Phase
0
10
20
30
40
50
60
70
0.0
0.5
1.0
1.5
2.0

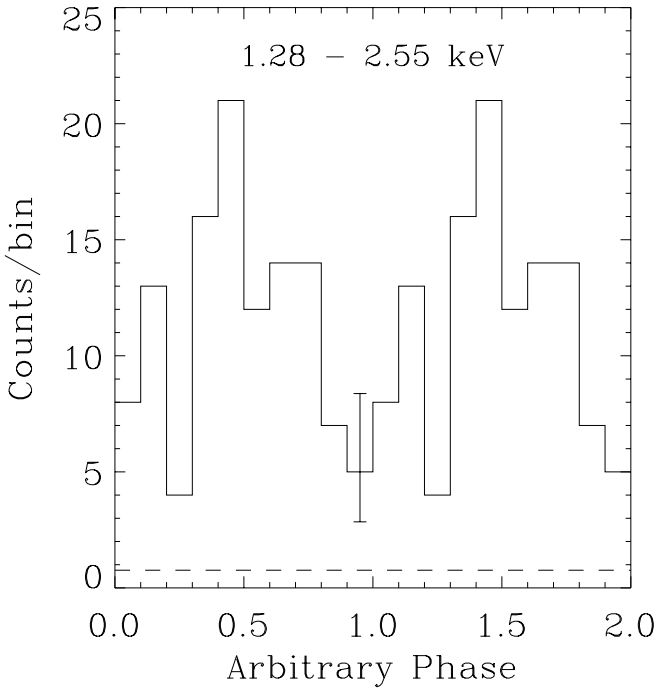
1.28 – 2.55 keV
Counts/bin
Arbitrary Phase
0
5
10
15
20
25
0.0
0.5
1.0
1.5
2.0

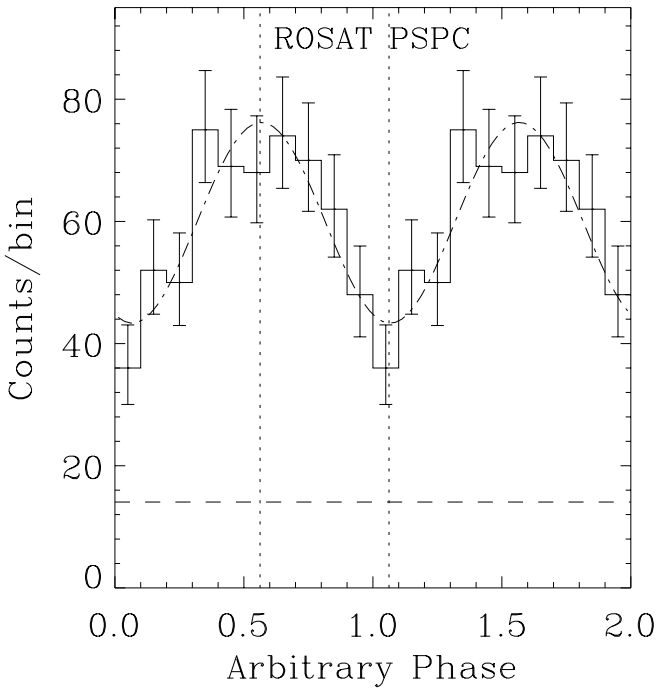
ROSAT PSPC
Counts/bin
0
20
40
60
80
0.0
0.5
1.0
1.5
2.0
Arbitrary Phase

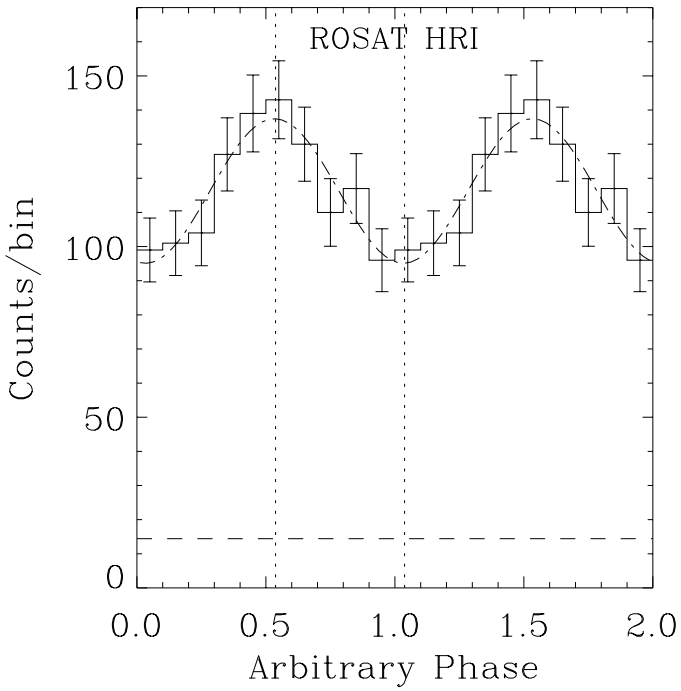
ROSAT HRI
150
100
50
0
Counts/bin
0.0
0.5
1.0
1.5
2.0
Arbitrary Phase

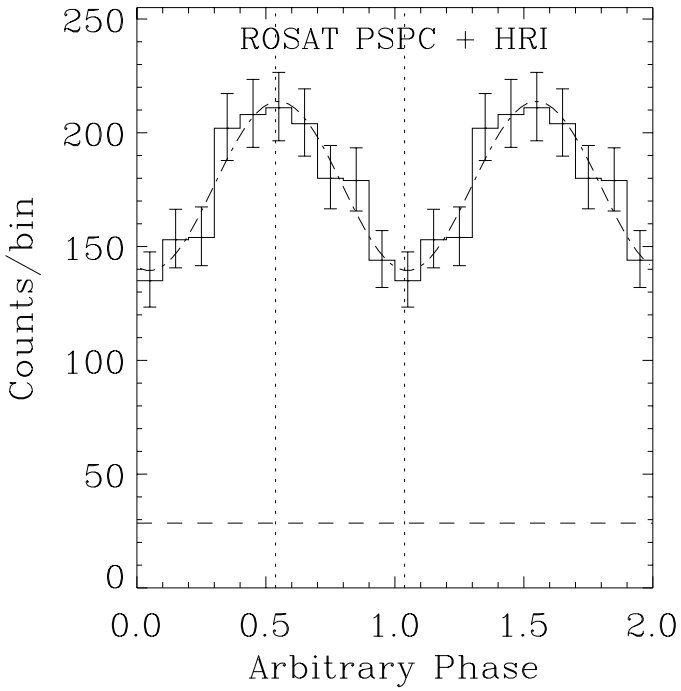
ROSAT PSPC + HRI
Counts/bin
250
200
150
100
50
0
0.0
0.5
1.0
1.5
2.0
Arbitrary Phase

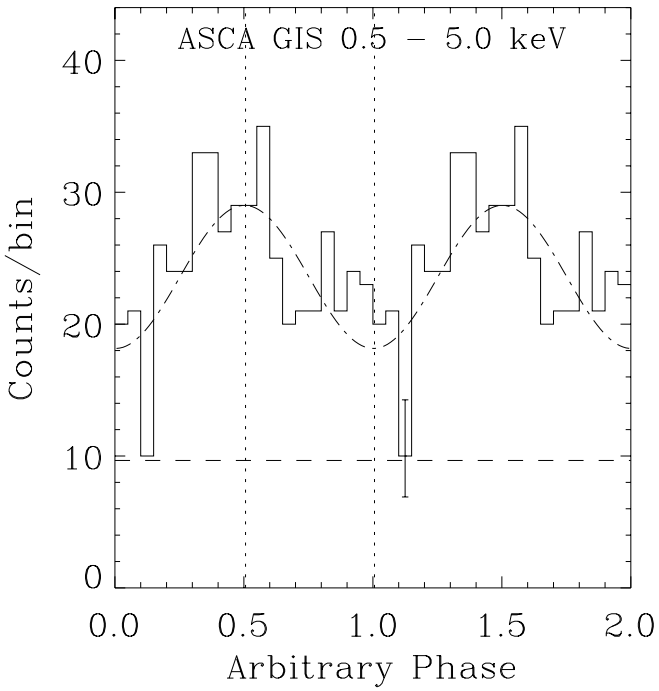
ASCA GIS 0.5 – 5.0 keV
Counts/bin
0
10
20
30
40
0.0
0.5
1.0
1.5
2.0
Arbitrary Phase

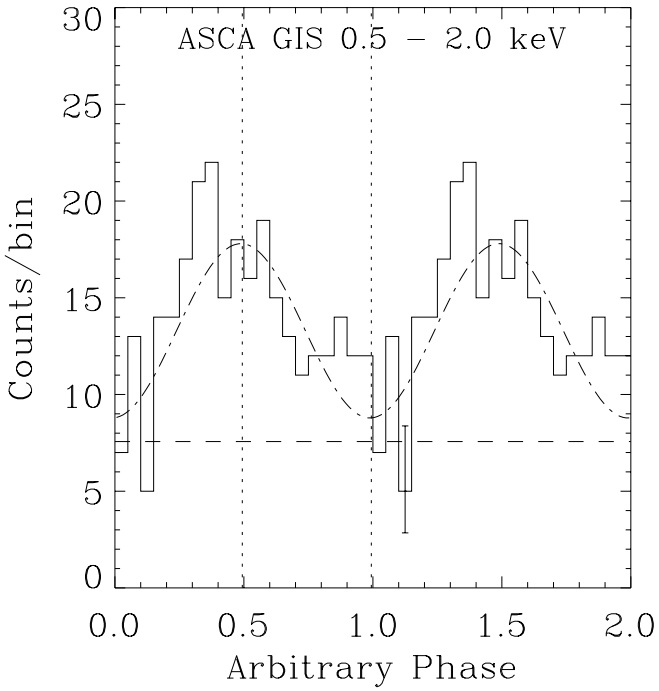
ASCA GIS 0.5 – 2.0 keV
Counts/bin
Arbitrary Phase
0
5
10
15
20
25
30
0.0
0.5
1.0
1.5
2.0

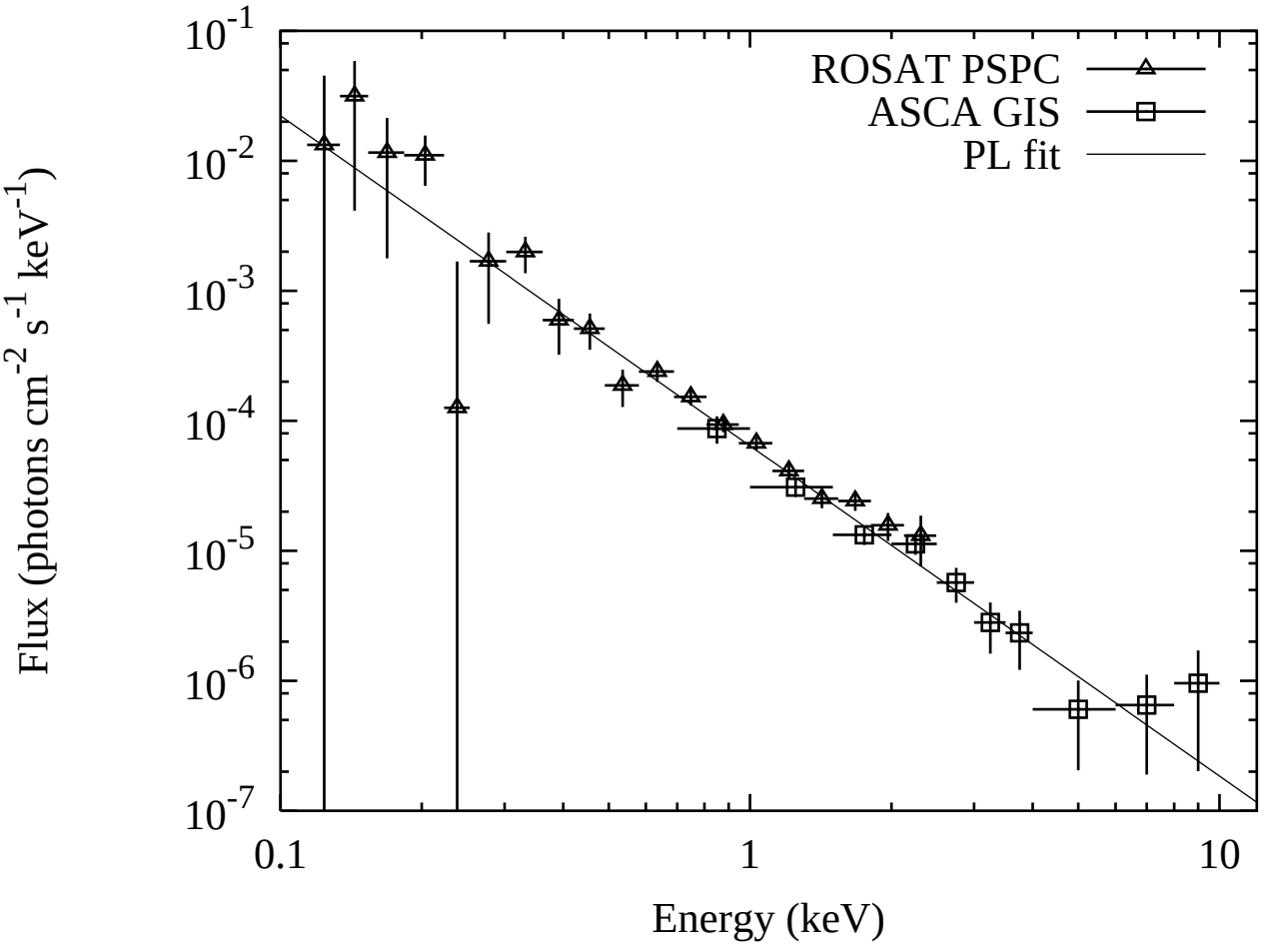
ROSAT PSPC
ASCA GIS
PL fit
Flux (photons cm^{-2} s^{-1} keV^{-1})
Energy (keV)
10^{-1}
10^{-2}
10^{-3}
10^{-4}
10^{-5}
10^{-6}
10^{-7}
0.1
1
10